Influence of ore size on the production of micro-sized ore particles by high-pressure gas rapid unloading

Genghao Zhang [a], Yongbo Fan [b], Renshu Yang [a,*], Shihai Li [b]

[a] School of Civil and Resource Engineering, University of Science and Technology Beijing, Beijing 100083, China
[b] Key Laboratory for Mechanics in Fluid Solid Coupling Systems, Institute of Mechanics, Chinese Academy of Sciences, Beijing, 100190, China

HIGHLIGHTS

- Applicate the GRU on kaolin pulverization.
- The gas infiltration stability time shows a squared relationship with increased ore size.
- Once the gas seepage thoroughly, extended infiltration times don't promote ore pulverization.
- Overall effect of pulverization is comparable for different ore sizes.

GRAPHICAL ABSTRACT
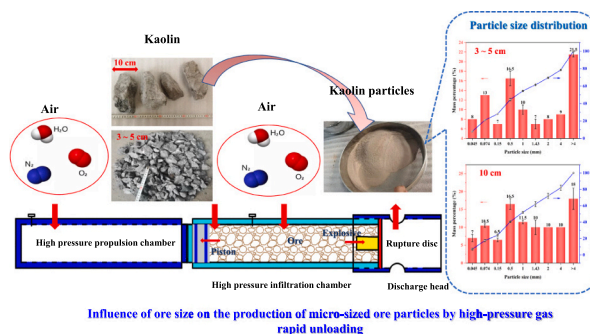
Influence of ore size on the production of micro-sized ore particles by high-pressure gas rapid unloading

ARTICLE INFO

ABSTRACT

Comminution of ore is a critical and energy-intensive process in mineral resource utilization. High-pressure gas rapid unloading (GRU) has emerged as a promising ore grinding technique, wherein high-pressure gas is injected into the ore and is unloaded at high speed to induce tensile failure inside the ore. Although the GRU is capable to achieve more efficient ore comminution with lower energy consumption compared to conventional methods, it is still in the early stages of development. The pulverization effect of different size ores is a crucial question needing to be revealed before the GRU industrial application. This study explores the impact of ore size on ore pulverization by GRU, using kaolin as an experimental material. Specifically, we discuss the following: 1. the impact of ore size on high-pressure gas infiltration, 2. the effect of infiltration time on ore pulverization, and 3. the effect of ore size on GRU-pulverized ore. The results indicate that the GRU pulverization method is highly applicable to kaolin, and different ore sizes have minimal effects on ore pulverization. Finally, we explain the insignificant size effect of GRU-pulverized ore by discussing the ore material length scale, deformation scale, and ore size. The conclusion may provide a basis for extending the GRU method from the experimental lab scale to a larger one. It may also provide a reference for applying GRU in kaolin comminution.

1. Introduction

The growth and development of human society rely heavily on the utilization of mineral resources. As social productivity continues to increase, the scale of mineral utilization has subsequently increased. In fact, the total amount of minerals mined in the latter half of the 20th century exceeds the total mining history recorded for thousands of years [1–3]. Comminution of ore is a critical upstream stage in the entire industrial process, as all ores, except for coastal sand mines, must undergo this process before further utilization. Multi-stage grinding technology combined with a ball mill is currently the mainstream ore pulverization technology [4]. Although mature enough to meet industrial production requirements, ore comminution remains an energy-intensive field [5]. According to statistics, ore comminution utilizes more than half of the electric energy used in mine production, consuming about 10% of global electricity production annually [6,7]. Given the Paris Association agreement in 2016, energy conservation and emission reduction have become a worldwide trend [8]. It is urgent to develop new energy-saving and efficient ore grinding technology.

Recently, several innovative grinding methods have emerged, including radio-frequency, high-voltage electric pulse, high-pressure water jet, etc. [9–13]. However, due to their insufficient processing capacity and high energy consumption, these methods are typically utilized as pretreatment technologies before ore grinding [14]. High-pressure gas rapid unloading (GRU) is an emerging ore pulverization technology. This method applies loading on the crystal scale by injecting high-pressure gas into the ore. As high-pressure gas rapid unloading, inducing ore occurs tensile failure from within and pulverizing ore into micron-sized particles in milliseconds [15–18]. The energy consumed by the tensile failure of ore and rock materials is only about 1/10 of that of extrusion failure [19]. Thus, GRU exhibits the potential to significantly reduce the ore comminution energy consumption compared to traditional methods. Table 1 portrays a mechanism comparison of several grinding machines. While extensive research has been conducted, GRU is still in the early stages of development. Lab-scale experiments have shown promising results, but further research is required for industrial-scale applications. Ore is a typical discontinuous and uniform material with a significant size effect [19,20]. The pulverization effect is likely to vary significantly to different size ores. Thus, studying the impact of ore

size on the grinding effect of GRU is crucial for promoting the GRU ore pulverization technology from laboratory to industrial scale.

Kaolin is a type of clay mineral that possesses excellent physical and chemical properties, including good plasticity, cohesiveness, insulation, acid resistance, and fire resistance. It has wide applications in ceramic, paper, refractories, cement, national defense, and other fields [21–24]. Despite being impacted by the novel coronavirus from 2021 to 2022, global kaolin production is still reaching 45 million tons [25]. The comminution process plays a crucial role in kaolin utilization, with the two mainstream methods being mechanical pulverization and jet milling. The conventional technique for kaolin pulverization involves multi-stage crushing and grinding mills, such as the Raymond mill, which is suitable for processing kaolin with high raw ore whiteness and low grit content [26]. However, the mechanical comminution process may increase the iron content in the crushed product or introduce other impurities. In contrast, the jet mill works by accelerating a high-pressure gas through a nozzle, which drives the material particles and causes them to crush, grind, and impact. The Jet mill hardly introduces impurities during the grinding process, making it suitable for fields that require high purity [27,28].
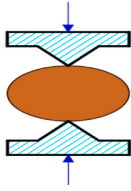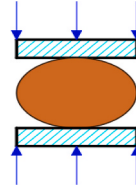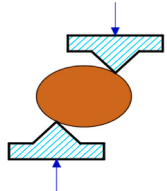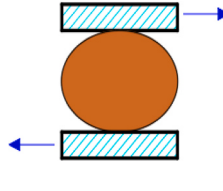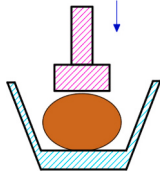
This paper uses kaolin to analyze the influence of ore size on the pulverization effect of GRU while clarifying the applicability of GRU to kaolin crushing. The following three issues are revealed in this paper: 1. The influence of ore size on high-pressure gas infiltration. 2. The influence of high-pressure gas infiltration time on ore pulverization. 3. The influence of ore size on the ore pulverization, given sufficient gas infiltration.

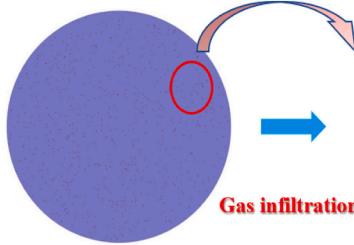## 2. Influence of ore size on high-pressure gas infiltration

2.1. Numerical simulation method and model

The high-pressure gas injected into the ore provides energy for GRU pulverizing the ore. The degree of gas infiltration into the ore directly affects the ore pulverization. According to the law of Darcy, the time required for complete gas infiltration in the ore is affected by ore size [29]. In order to clarify the influence of ore size on pulverization, the impact of ore size on high-pressure gas infiltration is firstly investigated. Since direct experimental observation is difficult, we analyze the process
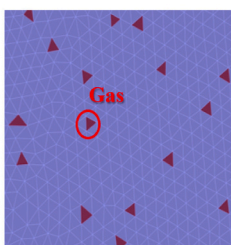
Table 1
The grinding mechanism of different comminution machine.

Destruction Mechanism	a. Split	b. Crush	c. Bend	d. Grinding	e. Impact
Jaw crusher	√	√	√	×	×
Cone crusher	×	√	√	×	×
Raymond Mill	×	√	×	√	√
Jet mill	×	√	×	√	√
Gas rapid unloading					
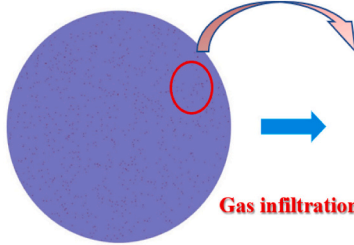
of high-pressure gas infiltration into the ore through numerical simulation using GDEM software which is based on the Continuous-Discontinuous Element (CDEM) algorithm [30–32]. Different sizes of ore are represented by establishing hemisphere models with different diameters. Several monitoring points are set in the hemisphere to record the change of infiltration pressure at specific positions. The infiltration model of ore is depicted in Fig. 1, while Fig. 2 shows the location of monitoring points in the ore model.

The calculation model includes multiple parameters in addition to ore size, including porosity, permeability, fluid viscosity, density, and infiltration pressure. Permeability and porosity of kaolin were measured using Pulse Attenuation and Gas Porosity measurements, respectively [33–37]. The porosity and permeability test instrument diagram are shown in Figs. 3 and 4. Detailed calculation parameters are illustrated in Table 2.

2.2. Numerical simulation implementation

After the injection of high-pressure gas, the pressure within the infiltration chamber quickly becomes constant. A constant pressure boundary condition at the hemispherical boundary represents the high-pressure gas environment. The calculation will terminate once the model central pressure equals the boundary pressure of 15 MPa. At that time, it is considered that high-pressure gas thoroughly permeates the ore. After the calculation, draw the infiltration pressure history curve as demonstrated in Fig. 5 a)-c). Fig. 5 d) illustrates the relationship between gas infiltration stabilization time and kaolin size.

Fig. 5 a-c) indicate that the gas pressure at the monitoring point is initially 0, and only increases once the high-pressure air infiltrates the area. As the gas infiltrates the ore, the pressure gradient between the internal part and the boundaries of the ore decreases, resulting in a reduced infiltration velocity. Consequently, pressure variation at the monitoring point decreases over the same time interval. Infiltration time at 15 MPa pressure increases as the ore size increases. Specifically, the time required for high-pressure gas infiltration stability increases from 2.2 min for 3 cm ore size to 6.2 min for 5 cm ore size and 24.9 min for 10 cm ore size. Numerical calculations demonstrate that the 15 MPa high-pressure gas can entirely infiltrate into −10 cm kaolin within 25 min. It is worth noting that the high-pressure gas has already begun to infiltrate into the ore before the pressure in the infiltration chamber stabilizes. However, numerical simulations often neglect this process, resulting in a slightly longer stability infiltration time than the actual occurrence. Additionally, the gas infiltration stability time exhibits a quadratic relationship with the increase in ore size. In particular, as the kaolin size increases in the ratio of 3:5:10, the infiltration stability time increases in the proportion of 9:25:100. These conclusions provide valuable
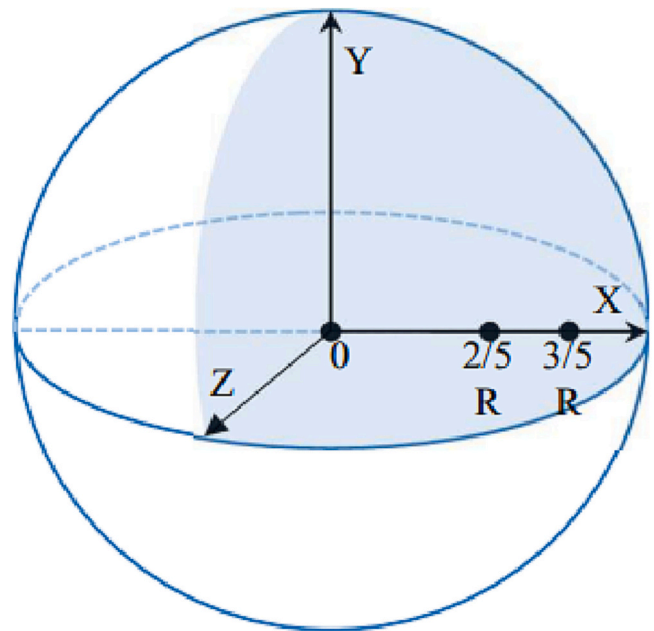

Fig. 2. Location of pressure monitoring points.

references for controlling the duration of high-pressure gas seepage in subsequent experiments.

3. Influence of high-pressure gas infiltration time on ore pulverization

3.1. Experimental methods

At an infiltration pressure of 15 MPa, numerical calculations indicate that the stabilization time for infiltration of 10 cm kaolin is <30 min. Theoretically, increasing the infiltration time should not affect the ore pulverization, provided that high-pressure gas infiltration is sufficient. Nonetheless, to be convincing, the numerical calculation outcomes must be confirmed by actual experiments. Accordingly, we subjected 10 cm of kaolin in the infiltration chamber to different times of infiltration 30, 90, and 120 min prior to rapidly unloading the gas. The particle size distribution (PSD) is crucial for particles, as it determines the quality, safety, and performance of the final product [38–40]. Analyzing PSD obtained at different infiltration time could demonstrate whether 15 MPa high-pressure gas fully infiltrates 10 cm kaolin.

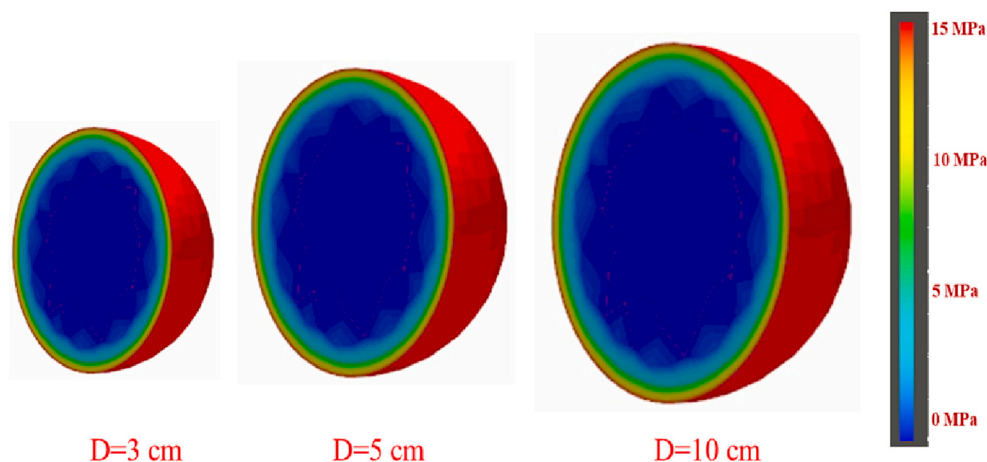The experimental apparatus for ore pulverization comprises a high-

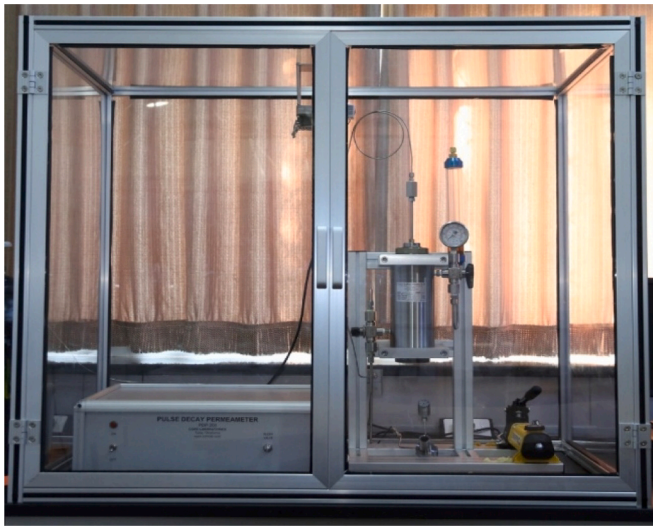**Fig. 1.** Calculation models for ores of different sizes.

Fig. 3. PDP 200 pulse decay permeability instrument.

Fig. 4. Porosity measurement system.

Table 2
The calculation parameters of gas infiltration.

Ore size (cm)	Porosity (%)	Infiltration pressure (MPa)	Permeability (10^{-9} D)	Aerodynamic viscosity (10^{-5} Pa·s)	Air density (kg/m^3)
3	0.63	15	15	2.22	177.88
5	0.63	15	15	2.22	177.88
10	0.63	15	15	2.22	177.88

pressure infiltration chamber and a high-pressure propulsion chamber. The rupture disc separates the infiltration chamber from the atmosphere, while the piston separates the infiltration chamber from the propulsion chamber. The high-pressure gas inside the propulsion chamber facilitates the kaolin to spout out of the infiltration chamber rapidly once the rupture disc ruptures. A schematic diagram of the experimental apparatus is shown in Fig. 6.

The experiment comprises four stages. First, the ore is placed into the high-pressure infiltration chamber. The explosive is attached to the rupture disc to instantly rupture the disc and achieve high-speed unloading of the infiltration chamber. Next, high-pressure gas is injected into both the infiltration and propulsion chambers. The high-pressure gas slowly infiltrates the pores in the ore until the gas pressure inside reaches equilibrium with the infiltration pressure. In the third stage, connect the wires to detonate the explosive charge adhered to the rupture disc. The rupture disc bursts leading to rapid unloading of the infiltration chamber, the ore rejecting with high-pressure airflow. In this stage, the ore is pulverized into micro-sized particles within milliseconds. The fourth and final stage involves removing the ore powder from the collection chamber and screening it. For further details about the experiment, refer to the paper [15–18].

The process of ore ejecting with the high-pressure airflow is the crucial stage to induce ore pulverization. During the ejecting process, gas pressure outside the kaolin drops significantly faster than inside the internal pores forming a high-pressure gradient. When the pressure gradient is large enough will overcome the tensile strength between ore particles, the kaolin chalks from within.

3.2. Experiment implementation and result analysis

We conducted experiments allowing 10 cm kaolin to stand in the infiltration chamber for 30, 90, and 120 min. The infiltration pressure and propulsion pressure were set at 15 MPa and 20 MPa, respectively. The mass of kaolin for each experiment is approximately 2000 g, with a size of about 10 cm. It is worth noting that due to the maximum diameter of the infiltration chamber being 10 cm, the diameter of the cross-section of the ore must not exceed 10 cm. However, the length of the ore may exceed 10 cm and even approach 15 cm. For more comprehensive information on the experimental parameters, please refer to Table 3. Follow the methodology outlined in section 3.1 to execute the experiment. Fig. 7. illustrates the experimental setup for ore pulverization.

Finally, open the collection container, remove the kaolin powder, Screen the kaolin powder, and draw the particle size distribution curve. The kaolin for experimentation and the kaolin powder after the experiment is illustrated in Fig. 8. The PSD of the kaolin powder obtained at different infiltration time is shown in Fig. 9.

The results presented in Fig. 9 reveal that extended infiltration time did not significantly increase the production of fine particles. At the infiltration times of 30, 90, and 120 min, −0.5 mm particles accounted for 40%, 41%, and 41%, respectively. The proportion of −74 μm particles in the three groups only fluctuated slightly. Similarly, the mass proportion of +2 cm coarse particles showed no regular changes. However, the mass ratio of 2–4 cm coarse particles decreased as the infiltration time increased. And the mass proportion of +4 mm coarse particles also decreased. The unpredictable nature of the ore's structure and experimental errors inevitably result in differences within local size intervals. Nonetheless, extending the infiltration time beyond 30 min had little effect on the overall kaolin pulverization. These experimental results shed light on two significant discoveries. Firstly, GRU is an effective technique for kaolin pulverization, generating approximately 40% -0.5 mm fine particles in a single comminution cycle. Secondly, high-pressure air at 15 MPa can fully infiltrate 10 cm of kaolin within 30 min. Furthermore, as long as infiltration is complete, prolonging the infiltration time does not significantly influence kaolin pulverization.

4. The influence of ore size on the ore pulverization

4.1. Experment implementation

Both experimental and numerical simulation results indicate that high-pressure air at 15 MPa can infiltrate 10 cm of kaolin within 30 min. To investigate the influence of ore size on the GRU pulverization effect, we further conducted two sets of pulverization experiments on kaolin with sizes of 3–5 cm and 10 cm, respectively. The gas infiltration pressure and propulsion pressure for the experiments are 15 MPa and 20 MPa, respectively. Table 4 presents the detailed experimental
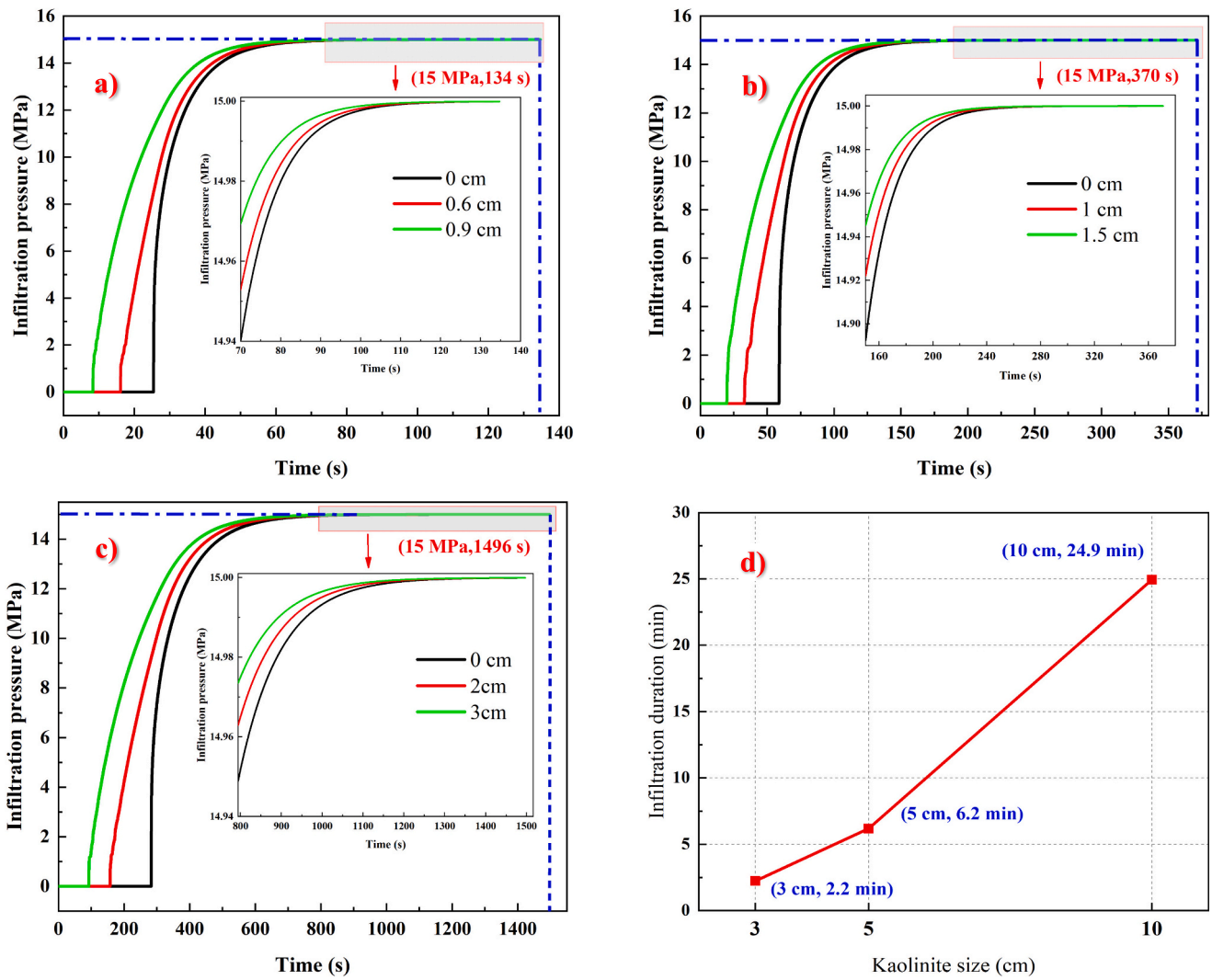
Fig. 5. Time gas infiltration time history curve of kaolin with different sizes. A). 3 cm. b) 5 cm c) 10 cm d) Gas infiltration stability time of kaolin with different sizes.

Fig. 6. Schematic diagram of the experiment apparatus.

parameters.

After experimenting, the effect of kaolin particle size on the efficiency of GRU pulverization was assessed by analyzing the PSD of the kaolin powder. The particle size distribution of kaolin with different sizes after pulverization is shown in Fig. 10.

Table 3
Experimental parameters.

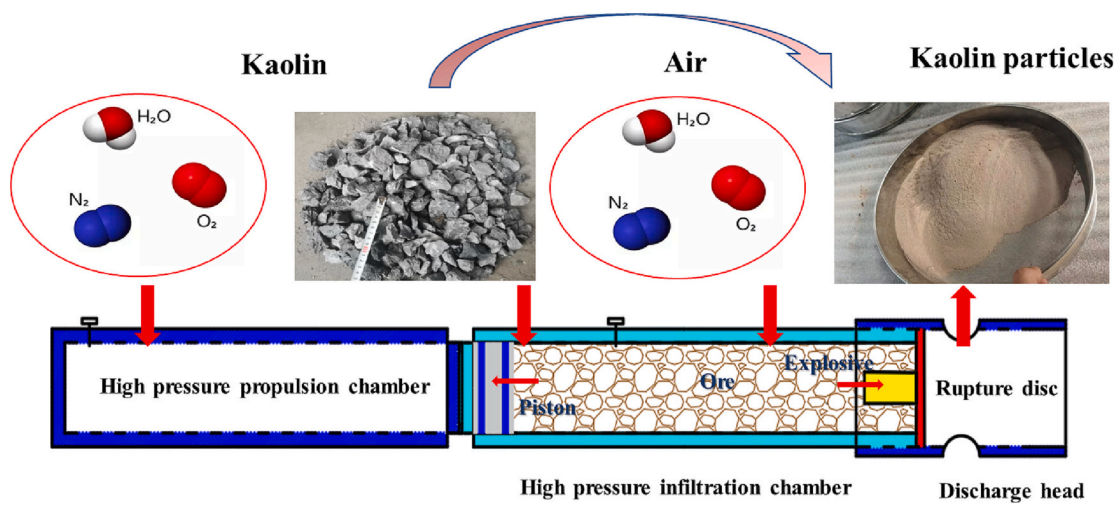| Parameters	Group 1	Group 2	Group 3
Weight (g)	2000	2000	2000
Kaolin size (cm)	10	10	10
Infiltration gas pressure (MPa)	15	15	15
Infiltration time (min)	30	90	120
Propulsion gas pressure (MPa)	20	20	20
The thickness of the rupture disk (mm)	4	4	4

4.2. Correlation analysis of the ore size and particle size distribution

Based on the experimental data, the results of the kaolin pulverization experiment exhibit a high level of stability at the infiltration pressure of 15 MPa. In the 3–5 cm kaolin pulverization experiment, the maximum deviation at 0.15–0.5 mm is approximately 1.5%. Similarly, the ultimate deviation of the 10 cm kaolin pulverization experiment occurs in the +4 mm block size, representing only a 1.5% deviation. At an infiltration pressure of 15 MPa, the pulverization effect of different sizes of kaolin is similar. Both 3–5 cm and 10 cm kaolin pulverization produce approximately 40% of particles with a size of −0.5 mm. However, examining specific particle size intervals, small-sized kaolin pulverization yielded slightly more fines and a slightly higher quantity of remaining coarse particles. For instance, 3–5 cm kaolin pulverization produced 1%, 2.5%, and 0.5% more particles of −45 μm, 74 μm, and

150 μm than 10 cm kaolin pulverization. Additionally, the coarse particles of +4 mm produced by crushing 10 cm kaolin were 4% less than that of 5 cm kaolin.

In conclusion, pulverization of small-sized kaolin by GRU produces slightly more fine particles and fewer coarse particles. However, overall, the pulverization efficiency of GRU on ores of different sizes is comparable without exhibiting noticeable size effects (SEs). These findings are significant and warrant further research and discussion.

5. Result and discussion

5.1. Results

This study investigates the effect of ore particle size on the crushing efficiency of GRU using kaolin as the experimental material. The numerical simulation results indicate that a 15 MPa high pressure can effectively infiltrate 10 cm kaolin within 30 min. The time required for gas infiltration prolongs in a quadratic relationship with the ore size increase. Furthermore, the experimental results demonstrate that continuously extending the infiltration time after adequate gas infiltration does not significantly improve the GRU pulverization efficiency of kaolin. Specifically, Fig. 9 depicts that at 15 MPa pressure, GRU pulverization produced about 40% of −0.5 mm particles after infiltration times of 30, 90, and 120 min. Lastly, experiments conducted on varying sizes of kaolin show that, even though small-sized kaolin generated

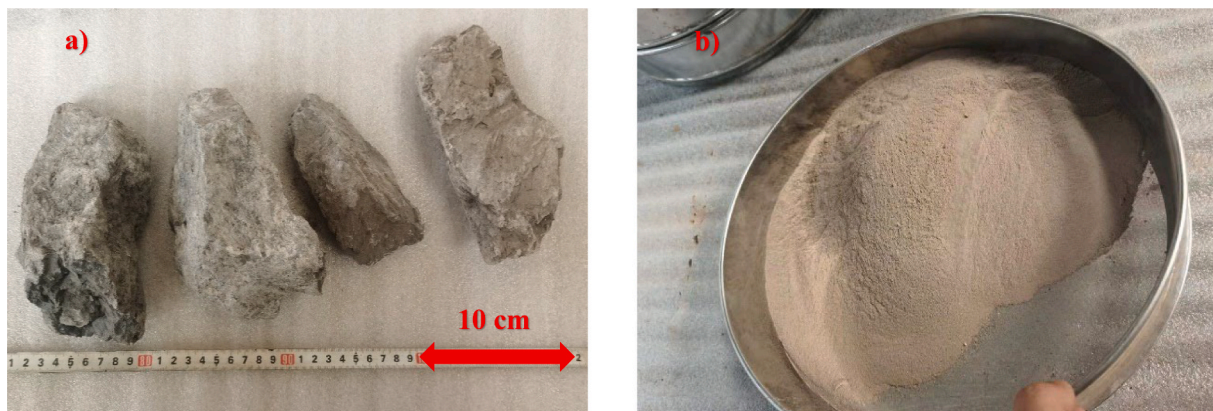

Fig. 7. Platform for ore pulverization.

Fig. 8. Kaolin before and after experiment. (a) Kaolin. (b) Kaolin powder.
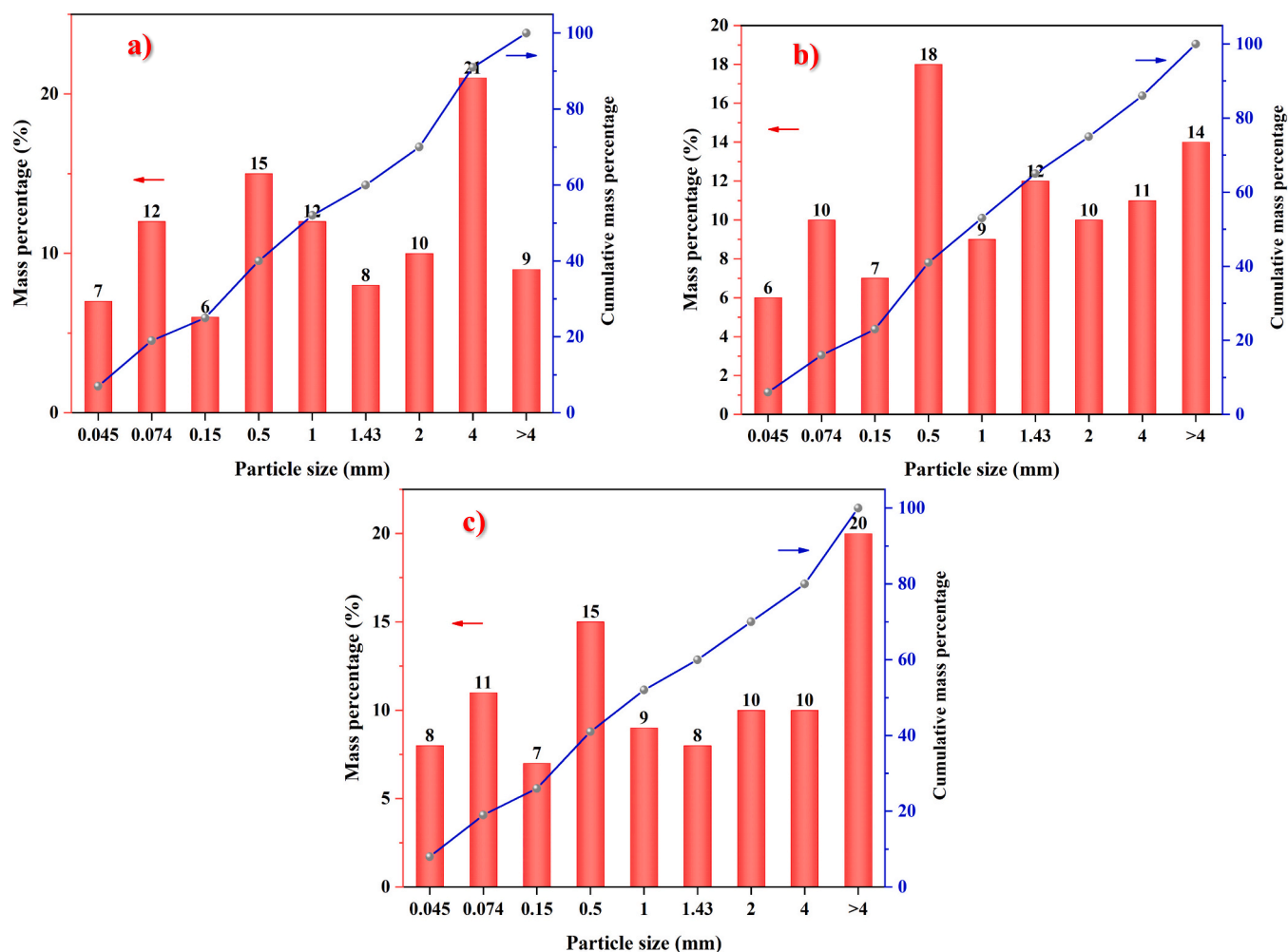
Fig. 9. Kaolin particle size distribution at different gas infiltration time. a) 30 min, b) 90 min, d) 120 min.

Table 4
Experimental parameters.

Parameters	Group 1	Group 2	Group 3	Group 4
Weight (g)	2000	2000	2000	2000
Kaolin size (cm)	3–5	3–5	10	10
Infiltration gas pressure (MPa)	15	15	15	15
Propulsion gas pressure (MPa)	20	20	20	20
Infiltration time (min)	30	30	30	30
The thickness of the rupture disk (mm)	5	5	5	5

slightly more fine powder and coarse particles than large-sized ones, the effect of GRU pulverization is comparable. At a 15 MPa infiltration pressure, 3–5 cm and 10 cm kaolin generated approximately 40% of −0.5 mm particles produced by GRU pulverization.

In summary, the study demonstrates that GRU technology can process various ore sizes and has the potential to be scaled up from a laboratory to an industrial production level. The GRU can be effectively integrated with existing ore crushing and grinding processes. Mined ores can be processed directly by the GRU without the need for pre-screening or secondary crushing. And the portion of the GRU grinding product that meets the selection criteria can be pre-screened and the remaining coarse particles can also meet the required feed size for further grinding. The GRU could increase ore grinding efficiency, reduce energy consumption and serve as a key technology for the mineral processing industry.

5.2. Discussion about the generalizability of the results

Experiments on kaolin pulverization have indicated that GRU pulverization is not significantly affected by the size of the ore. However, it is hasty to draw such a conclusion based on a single type of ore. To verify this finding, we conducted additional experiments using iron ore as the material. The gas infiltration and propulsion pressures were maintained at 15 MPa and 20 MPa, respectively. Each experiment involved a mass of approximately 2000 g of iron ore with sizes of around 3–5 cm and 10 cm. After the experiments, according to the PSD to analyze the influence of iron ore size on GRU pulverization. Fig. 11 illustrates the iron ore before and after the experiment.

The results presented in Fig. 12 demonstrate that the effect of pulverizing 10 cm iron ore with GRU is comparable to that of 3–5 cm iron ore at an infiltration pressure of 15 MPa. Both 3–5 cm and 10 cm iron ores produce 39% and 41% of particles measuring −0.5 mm, respectively. Moreover, the yield of −150 μm particles in both cases is 29%. Meanwhile, 3–5 cm iron ore pulverization by GRU produces 4% and 8% >10 cm of −45 μm fine particles and coarse particles of +4 mm, respectively. The conclusion obtained by different sizes of iron ore pulverization experiments is consistent with kaolin. Although the GRU pulverizes small-sized ores and produces slightly more fine and coarse particles, the overall effect of ore pulverization remains comparable to that of large-sized ore. The size effects on ore pulverized by GRU are negligible.
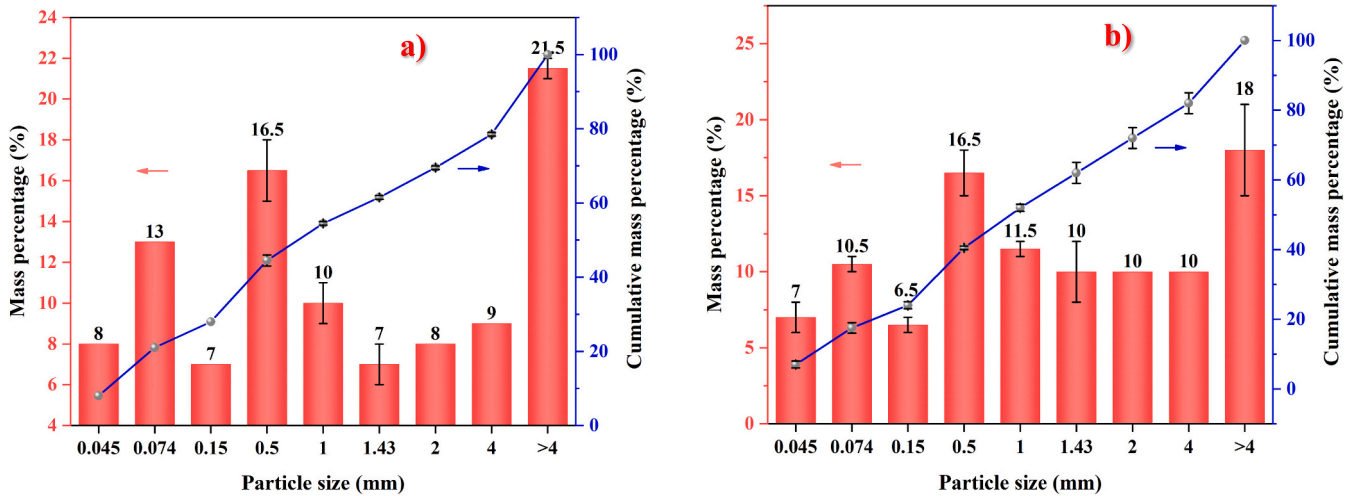
Fig. 10. Particle size distribution of different sizes kaolin pulverization obtained at infiltration pressure of 15 MPa.a) 3–5 cm b) 10 cm.

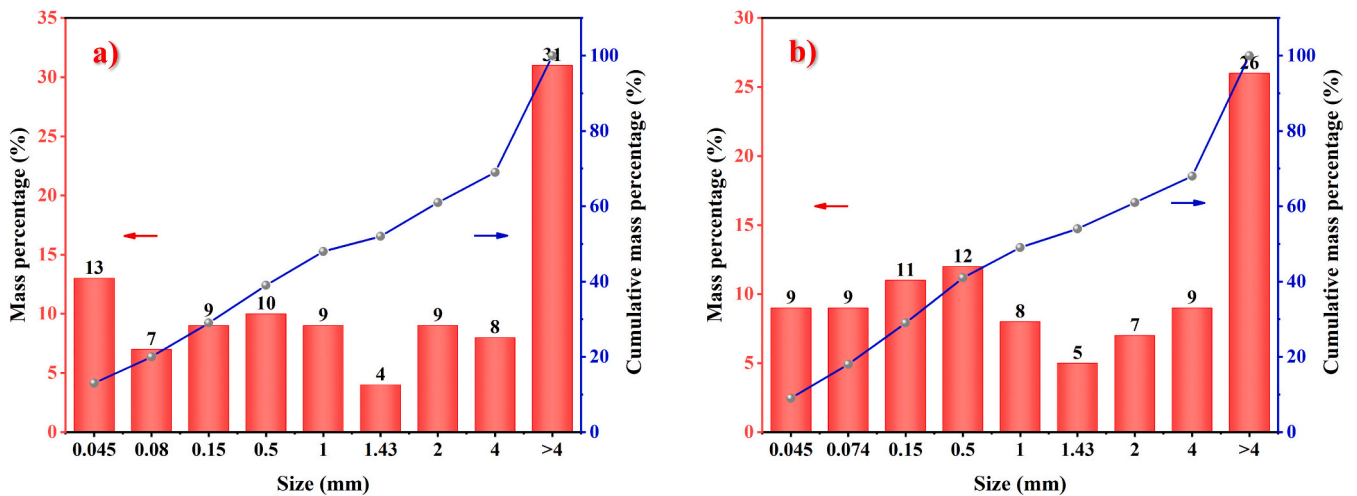**Fig. 11.** Iron ore before and after experiment. a) Iron ore. b) Iron ore powder.

Fig. 12. Particle size distribution of different sizes iron ore pulverization obtained at infiltration pressure of 15 MPa.a) 3– 5 cm b) 10 cm.

5.3. Discussion about the SEs on ore pulverization by GRU

The experiments on the pulverization of kaolin and iron ore have both demonstrated that GRU pulverizes ores of varying sizes with comparable efficacy. Meanwhile, it is also observed that pulverization of smaller ore sizes obtains slightly more fine and coarse particles. In this section, we discuss the underlying mechanisms. The ores ejected from the infiltration chamber inevitably collide with the discharge head, causing damage and generating coarse particles. Subsequently, the internal gas expansion induces ore pulverization from within.

Additionally, given a fixed mass of ores, the number of small-sized ores exceeds that of the large-sized ones. The likelihood of individual small-sized ores colliding with the discharge head is correspondingly lower than that of large-sized ores, which makes the small-sized ores pulverization generate more coarse particles compared to larger ones. However, for the same mass of ores, small-sized ones have a larger free surface area than large-sized ones. Therefore, the internal gas expansion is more likely to produce fine particles for small-sized ores. To reduce the remaining coarse particles from small-sized ores pulverization and increase the production of fine particles from large-sized ones, the following methods can be applied: 1. enlarging the outlet size of the soaking chamber to increase the probability of each small ore colliding with the discharge head, and 2. modifying the shape of the discharge head to facilitate sufficient collisions with large-sized ores, leading to more free surface area and increased production of fine particles from large-sized ores.

The pulverization efficiency of GRU on ores of different sizes is comparable without exhibiting noticeable size effects. This phenomenon deserves further examination through in-depth discussion. Size effects (SEs) are commonly observed in various domains of physics and engineering [20]. The SEs announcement is related to the specimen size, deformation scale, and internal material length scale. Usually, decreasing the size of a specimen results in a stronger response in several plasticity phenomena. For example, decreasing the size of the indenter increases the indentation hardness of metals and ceramics. The solid material hardening is assumed to result from accumulating statistically stored dislocations ρ_S and geometrically necessary dislocations ρ_G [41]. When the length scale associated with the deformation field is small compared to a material length scale, the density of geometrically necessary dislocations swamps the statistically stored ones, resulting in obvious size effects. For example: at 10% strain $\rho_G \gg \rho_S$ for $\lambda < 50$ μm in single crystals and for $\lambda < 20$ μm in polycrystals [42]. (λ represents the material length scale. In the torsion test, λ is simply the radius of the cylinder; in bending it is the half thickness of the beam; in the hardness test it is related to the indent size; at the crack tip, to the plastic zone size; In polycrystals one might expect it to be related to the grain size.) When the length scale associated with the deformation field is large enough, the $\rho_G \ll \rho_S$ and the conventional plasticity laws without length scale is sufficient. Considering a specific material with a defined material length scale, the SEs weaken as the deformation field increases. Fig. 13 illustrates that the hardness of cold-worked polycrystalline Cu and single-crystal Cu gradually stabilizes as the indentation depth exceeds 1 μm [43].
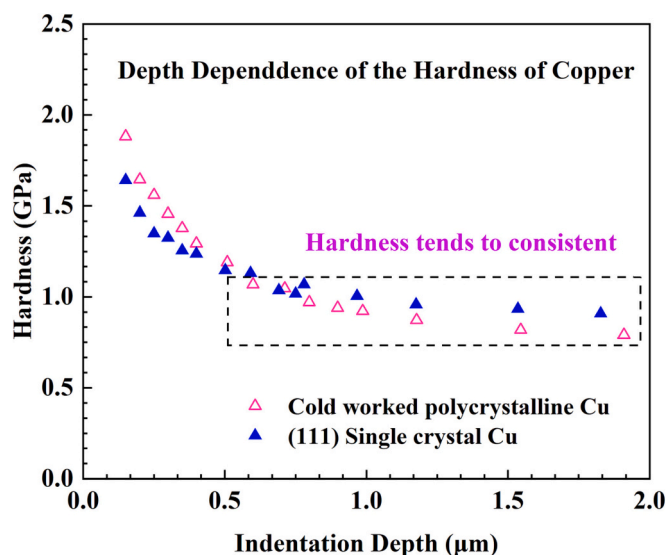

Fig. 13. The depth dependence of hardness copper.

For a given material with a defined material length scale, the specimen size becomes critical in the SEs. Ore and rock materials possess multi-scale micro-defects. Rocks exhibit a large range of SEs compared to metal materials, in magnitude up to macroscopic levels. It shows a "smaller, stronger" mechanical response, increasing strength with specimen size reduction. As the specimen size approaches the rock material length scale, the number of microstructures increases with increasing specimen size. Besides, micro-fractures become more likely to capture each other, accumulate, and eventually form macroscopic cracks. Therefore, rock materials demonstrate a significant size-dependent mechanical response within a certain size range. When the specimen size is large enough to contain sufficient micro-defects, the effects of local micro-defects on its apparent mechanical properties weaken. Its mechanical properties approach those of the rock mass, diminishing the corresponding size dependence. Fig. 14 describes the SEs of compressive strength of 6 kinds of ore rock materials [44]. Before 20 cm, the compressive strength of the six ore rocks decreased sharply with the specimen size increase. When the specimen size exceeds a particular value, the compressive strength of several ores tends to be consistent, respectively.

GRU employs high-pressure gas rapid decompression to induce ore pulverization on the single-crustal scale from within. The materials length scale associated with the GRU pulverized ores is on the crystal scale. The ore particles dissociate from the cemented status as the around cracks expand from pore initiation. The local mechanical response may differ due to the fracture density distribution and the inter-particle strength difference. The pulverization of ore by GRU results in deformations that not only occur at the crystalline scale but also extend to the macroscopic level, ultimately leading to the cross-scale destruction of the ore into powder particles. Such a large deformation scale swallows up the differences caused by local micro-defects. Furthermore, the macroscale ore already contains many randomly distributed microfractures. The regional microstructural differences have less weight on the overall mechanical response. Rock specimens with different macroscopic scales have the same microstructural characteristics. Therefore, changing the ore dimension does not significantly affect the overall ore pulverization effect.

5.4. Discussion about the application of GRU comminution technology in kaolin

The GRU has broad potential applications in the field of kaolin grinding. Firstly, it can simplify and revolutionize the existing kaolin-crushing technology. Experimental results have demonstrated that the GRU can effectively pulverize large-sized kaolin into fine powder. Pulverizing 10 cm kaolin using the GRU at an infiltration pressure of 15 MPa yields particles smaller than 2 mm at around 70% after one comminution cycle. Therefore, most of the mined kaolin can be directly fed into the grinding stage after the GRU process. Coarse particles that do not meet the mill feed size requirements will be recycled into the subsequent grinding cycle as sand returns. Secondly, the GRU can increase kaolin crushing efficiency, reduce grinding volume, and lower energy consumption. The GRU can crush kaolin into micro-sized particles in milliseconds, considerably reducing the cost of ore crushing time. As shown in Fig. 10, a single pulverization cycle produced nearly 30% of −150 μm particles. Pre-screening can separate the eligible fines, thereby reducing grinding volume. Lastly, the GRU utilizes high-pressure gas as the energy input, with no impurities introduced into the grinding product. Consequently, the purity of the final crushed product is improved compared to conventional mechanical methods.

Kaolin is a high-quality but limited resource in natural resource. The limited fine-grained content of the raw ore restricts the yield of high-quality kaolin products. To obtain fine-grained kaolin flakes, the deep processing of kaolin requires the flaking technique, which breaks down the coarse-grained crystals [24,45]. The mainstream kaolin splitting techniques include mechanical grinding, high-pressure extrusion, and
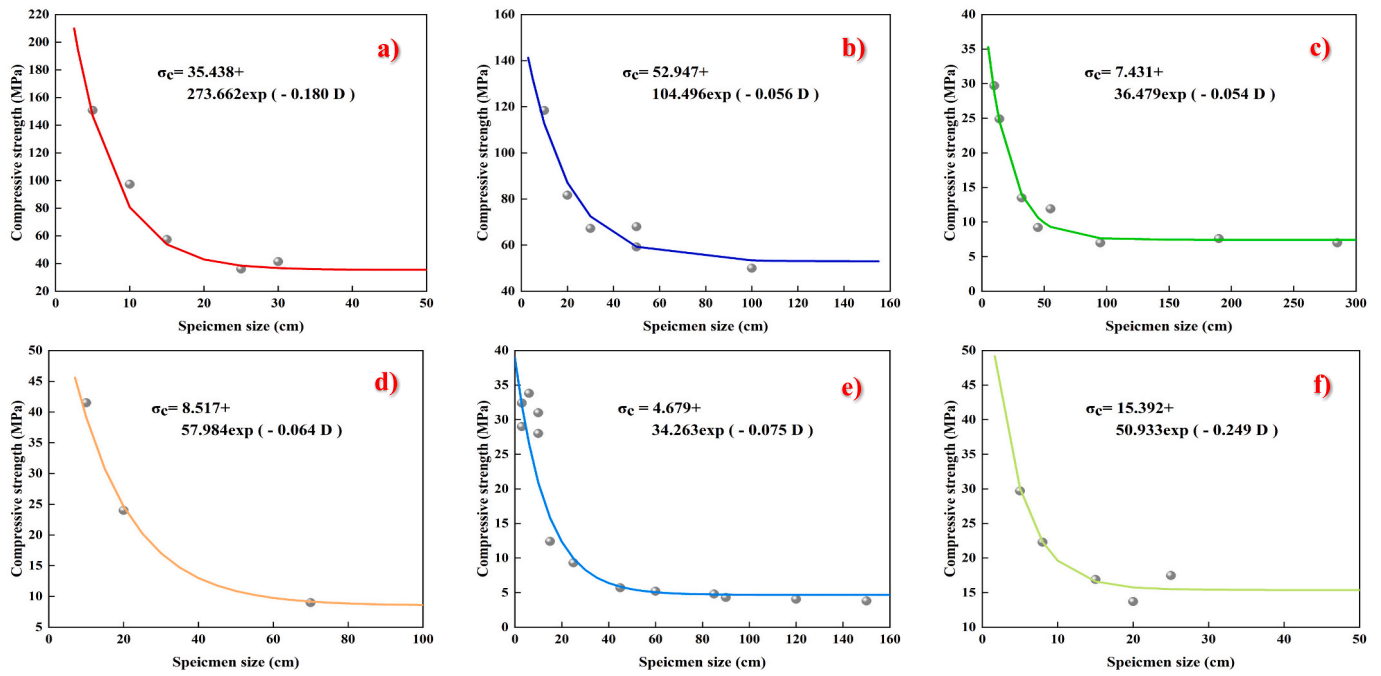
Fig. 14. Size effect for compression strength of several rocks. a). limestone. b). iron ore. c). diorite. d). quartz. e). coal. f). mica schist.

chemical soaking. The high-pressure extrusion method utilizes a high-pressure homogenizer to pressurize the kaolin and spout at high speed. The sudden decompression during the ejection causes the kaolin crystals to dissociate due to the impact, shear, and cavitation. GRU pulverized kaolin follows a similar mechanism to the high-pressure extrusion process, but pulverization happens in the gas phase. The high-pressure gas entering the kaolin layers may produce a better splitting effect after unloading and expansion, as shown in Fig. 15.

6. Conclusion

This paper investigates the impact of ore size on ore pulverization by the GRU. The research includes numerical simulations and experiments,

which show that high-pressure gas (15 MPa) completely infiltrates 10 cm kaolin in 30 min. The time for gas infiltration increases quadratic as the ore size increases. Specifically, as the kaolin size grows in the ratio of 3:5:10, the infiltration stability time extends in the proportion of 9:25:100. However, extending the infiltration time after adequate gas infiltration does not significantly improve the ore pulverization effect. At a 15 MPa pressure, GRU pulverization results in approximately 40% of −0.5 mm particles after infiltration times of 30, 90, and 120 min. The study also found that the GRU can pulverize ores of various sizes with similar effectiveness. At an infiltration pressure of 15 MPa, pulverization of 3–5 cm and 10 cm kaolin yields nearly comparable results, producing around 40% of −0.5 mm and 30% of −150 μm particles, respectively. The conclusion is corroborated by iron ore pulverization experiments,
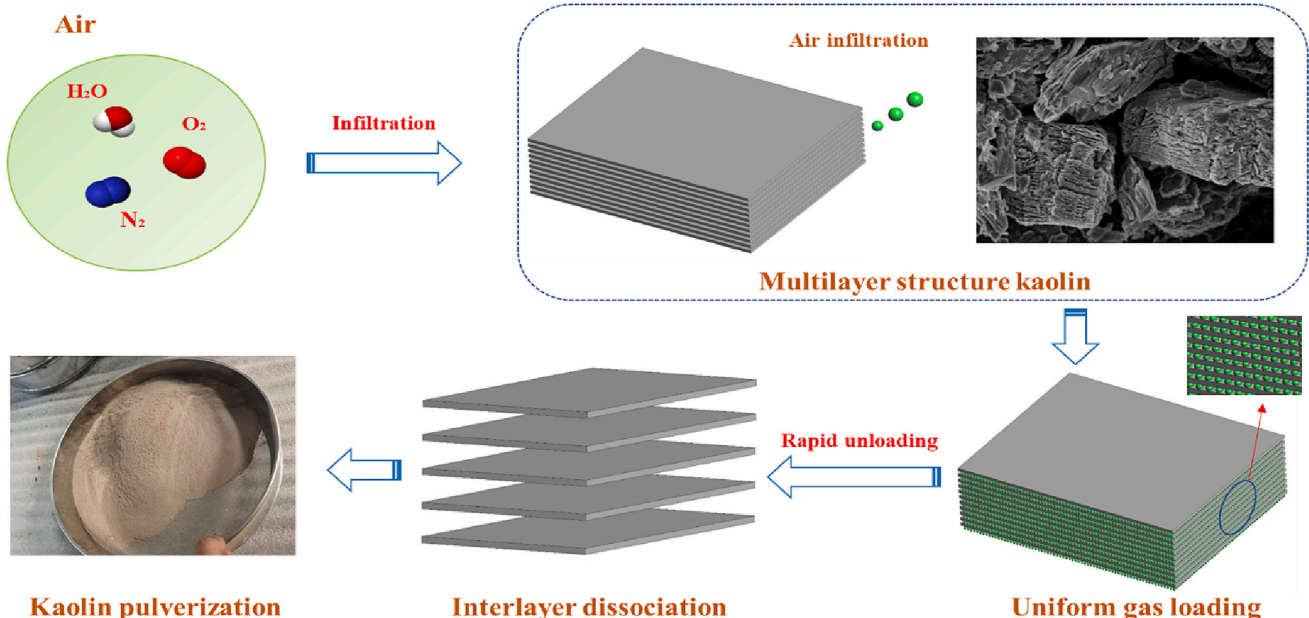

Fig. 15. Splitting mechanism of the GRU.

which show that the GRU produces similar results for different ore sizes.

The GRU applies uniform equal stress loading on the ore particle single crystal scale, inducing ore destruction from within. However, as ore pulverization by the GRU involves much larger deformation scales and specimen sizes than crystal scale, altering the ore size does not significantly impact the pulverization effect. This conclusion could serve as the basis for scaling up the GRU pulverization method from laboratory to industrial scale. Furthermore, it can provide an essential reference for subsequent GRU methods used in kaolin pulverization research.

CRediT authorship contribution statement

Genghao Zhang: Conceptualization, Investigation, Data curation, Writing – original draft, Writing – review & editing, Methodology, Formal analysis. **Yongbo Fan:** Methodology, Formal analysis, Writing – review & editing. **Renshu Yang:** Methodology, Supervision, Resources, Formal analysis, Funding acquisition. **Shihai Li:** Resources, Methodology, Writing – review & editing, Formal analysis.

Declaration of Competing Interest

The authors declare no competing interests.

Data availability

Data will be made available on request.

Acknowledgements

References

[1] International Mining Research Center, China Geological Survey, Global Mining Development Report 2019-2020, Beijing, 2020.
[2] BP, Statistical Review of World Energy, 2022, p. 2022.
[3] A.E. Eckes Jr., The United States and the Global Struggle for Minerals, University of Texas Press, 1979.
[4] D.N. Oleg, Mechanical Crushing and Grinding, Elsevier, Netherlands, 2019, pp. 65–90.
[5] P. Parisa, R. Jan Mehdi, Quantitative analysis of ore texture breakage characteristics affected by loading mechanism: fragmentation and mineral liberation, Miner. Eng. 182 (2022), 107561.
[6] J. Jack, S. Alex, Energy consumption in mining comminution, Procedia CIRP 48 (2016) 140–145.
[7] H. Kenneth, K.-R. Päivi, H. Pirita, V. Kati, E. Ali, Global energy consumption due to friction and wear in the mining industry, Tribol. Int. 115 (2017) 116–139.
[8] P. Agreement, Paris agreement, report of the Conference of the Parties to the United Nations Framework Convention on Climate Change 21st Session, 2015: Paris, Retrived December, HeinOnline, 2015, p. 2017.
[9] A. Swart, P. Mendonidis, Evaluating the effect of radio-frequency pre-treatment on granite rock samples for comminution purposes, Int. J. Miner. Process. 120 (2013) 1–7.
[10] L. Yan, W. Meirong, Z. Tao, Q. Hongchao, L. Hui, Overview on the development and critical issues of water jet guided laser machining technology, Opt. Laser Technol. 137 (2021), 106820.
[11] J.S. Carlton, Chapter 16 - Waterjet Propulsion, 2019, pp. 399–408.
[12] C.-G. Cho, H.-J. Ryoo, Design of Compact Solid-State Modulator for high-power electromagnetic pulse generation, IEEE Journal of Emerging and Selected Topics in Power Electronics 9 (5) (2021) 6059–6068.
[13] H. Wei, S. Fengnian, Selective breakage of mineralised synthetic particles by high voltage pulses. Part 2: interactions between mineralised particles in a multiple-particle system, Miner. Eng. 146 (2020) 106149.
[14] V. Singh, P. Dixit, R. Venugopal, K.B. Venkatesh, Ore pretreatment methods for grinding: journey and prospects, Miner. Process. Extr. Metall. Rev. 40 (1) (2019) 1–15.
[15] Z. Genghao, F. Yongbo, Y. Renshu, L. Shihai, Application of the rosin-Rammler function to describe quartz sandstone particle size distribution produced by high-pressure gas rapid unloading at different infiltration pressure, Powder Technol. 412 (2022), 117982.
[16] Y.B. Fan, J.Y. Qiao, S.H. Li, C. Feng, Micron-sized ore powder production by propulsion and rapid unloading of high-pressure gas, J. Aust. Ceram. Soc. 57 (5) (2021) 1489–1497.
[17] Y.B. Fan, J.Y. Qiao, S.H. Li, C. Feng, Micron-sized silicon carbide particle production via rapid unloading of high-pressure liquid CO 2, J. Aust. Ceram. Soc. 55 (2) (2019) 595–600.
[18] Y.B. Fan, W.J. Duan, S.H. Li, J.Y. Qiao, Experiment on micron-sized particle production of iron ore by rapid unloading of liquid CO2, Powder Technol. 327 (2018) 449–455.
[19] W. Zhi-Yang, L. Ying-Wei, W. Zhi-Jun, Hierarchical scaling model for size effect on tensile strength of polycrystalline rock, Int. J. Mech. Sci. 247 (2023), 108171.
[20] M.W. Fu, J.L. Wang, Size effects in multi-scale materials processing and manufacturing, Int. J. Mach. Tools Manuf. 167 (2021), 103755.
[21] P. Das, T.V. Bharat, Kaolin based protective barrier in municipal landfills against adverse chemo-mechanical loadings, Sci. Rep. 11 (1) (2021) 10354.
[22] H.M. Haydn, Chapter 5 kaolin applications, in: Developments in Clay Science 2, 2006, pp. 85–109.
[23] H. Yuan, T. Shengwei, Y. Shaohua, L. Shiwei, Research progress on green synthesis of various high-purity zeolites from natural material-kaolin, J. Clean. Prod. 306 (2021), 127248.
[24] L. Qinfu, L. Xiaoguang, C. Hongfei, Insight into the self-adaptive deformation of kaolinite layers into nanoscrolls, Appl. Clay Sci. 124-125 (2016) 175–182.
[25] U.S.G. Survey, Mineral commodity summaries 2022, in: Mineral Commodity Summaries, Reston, VA, 2022, p. 202.
[26] Niu Dan, Chen Xisong, Yang Jun, Z. Xingpeng, Disturbance rejection control for Raymond mill grinding system based on disturbance observer, J. Cent. South Univ. 24 (9) (2017) 2019–2027.
[27] A. Chamayou, J.A. Dodds, Air jet milling, in: Handbook of Powder Technology 12, 2007, pp. 421–435.
[28] L. Scott, A. Borissova, A. Burns, M. Ghadiri, Influence of holdup on gas and particle flow patterns in a spiral jet mill, Powder Technol. 377 (2021) 233–243.
[29] S. Whitaker, Flow in porous media I: a theoretical derivation of Darcy's law, Transp. Porous Media 1 (1986) 3–25.
[30] Z. Xinguang, F. Chun, C. Pengda, W. Xinquan, L. Shihai, A novel three-dimensional hydraulic fracturing model based on continuum–discontinuum element method, Comput. Methods Appl. Mech. Eng. 383 (2021), 113887.
[31] W. Chao, L. Yong, Z. Weishen, L. Shucai, W. Shugang, W. Hanpeng, Experimental observation and numerical investigation on propagation and coalescence process of multiple flaws in rock-like materials subjected to hydraulic pressure and far-field stress, Theor. Appl. Fract. Mech. 108 (2020), 102603.
[32] J. Yang, L. Peng, C. Jialiang, Y. Yongming, G.R. Pathegama, CDEM-based analysis of the 3D initiation and propagation of hydrofracturing cracks in heterogeneous glutenites, J. Nat. Gas Sci. Eng. 35 (2016) 614–623.
[33] H. Jeong, D.K. Hsu, Experimental analysis of porosity-induced ultrasonic attenuation and velocity change in carbon composites, Ultrasonics 33 (3) (1995) 195–203.
[34] I. Daniel, S. Wooh, I. Komsky, Quantitative porosity characterization of composite materials by means of ultrasonic attenuation measurements, J. Nondestruct. Eval. 11 (1992) 1–8.
[35] E.W. Washburn, E.N. Bunting, Porosity: VI. Determination of porosity by the method of gas expansion, J. Am. Ceram. Soc. 5 (2) (1922) 112–130.
[36] D. Yi, S. Shuxun, P. Zhejun, W. Wenfeng, L. Shiqi, F. Changqing, Z. Yongchun, Z. Junying, Experimental study of supercritical CO2-H2O-coal interactions and the effect on coal permeability, Fuel 253 (2019) 369–382.
[37] R. Danielson, P. Sutherland, Porosity, Methods of Soil Analysis: Part 1 Physical and Mineralogical Methods 5, 1986, pp. 443–461.
[38] A. Macias-Garcia, M.C.C. Eduardo, M.A. Diaz-Diez, Application of the Rosin–Rammler and Gates–Gaudin–Schuhmann models to the particle size distribution analysis of agglomerated cork, Mater. Charact. 52 (2) (2004) 159–164.
[39] B. Magnus, Empirical energy and size distribution model for predicting single particle breakage in compression crushing, Miner. Eng. 171 (2021), 107094.
[40] Ś. Grzegorz, M. Janusz, Forward and inverse analysis for particle size distribution measurements of disperse samples: a review, Measurement 187 (2022), 110256.
[41] J. Hutchinson, N. Fleck, Strain gradient plasticity, Adv. Appl. Mech. 33 (1997) 295–361.
[42] N. Fleck, G. Muller, M.F. Ashby, J.W. Hutchinson, Strain gradient plasticity: theory and experiment, Acta Metall. Mater. 42 (2) (1994) 475–487.
[43] K. McElhaney, J.J. Vlassak, W.D. Nix, Determination of indenter tip geometry and indentation contact area for depth-sensing indentation experiments, J. Mater. Res. 13 (5) (1998) 1300–1306.
[44] B.C. Liu, J.S. Zhang, Q.Z. Du, A study of size effect for compression strength of rock, Chin. J. Rock Mech. Eng. 06 (1998) 611–614.
[45] V.L. Bosazza, Textures of clays, Nature 147 (3738) (1941) 779.